Biophysical Chemistry 157 (2011) 7–15

Contents lists available at ScienceDirect

Biophysical Chemistry

journal homepage: http://www.elsevier.com/locate/biophyschem

Conformational heterogeneity and dynamics in a βγ-Crystallin from *Hahella chejuensis*

Atul K. Srivastava [1], Kandala V.R. Chary *

Department of Chemical Sciences, Tata Institute of Fundamental Research, Mumbai-400005, India

ARTICLE INFO

Article history:
Received 14 February 2011
Received in revised form 3 April 2011
Accepted 3 April 2011
Available online 9 April 2011

Keywords:
Conformational dynamics
Structural heterogeneity
Reduced spectral density mapping
Hahella chejuensis
Greek key
Curved temperature dependence

ABSTRACT

Most of the βγ-crystallins are structural proteins with high intrinsic stability, which gets enhanced by Ca^{2+}-binding in microbial members. Functions of most of these proteins are yet to be known. However, a few of them were reported to be involved in Ca^{2+}-dependent and stress-related functions. Hahellin, a microbial homolog, is a natively unfolded protein that acquires a well-folded structure upon Ca^{2+} binding. Although the structure of βγ-crystallin domains is well understood, the dynamical features are yet to be explored. We have investigated for the first time the equilibrium dynamics, conformational heterogeneity and associated low-lying free-energy states of hahellin in its Ca^{2+}-bound form using NMR spectroscopy to understand the dynamics of a βγ-crystallin domain. Hahellin shows large conformational heterogeneity with nearly 40% of the residues, some of which are part of Ca^{2+}-binding loops, accessing alternative states. Further, out of the two Greek key motifs, which together constitute the βγ-crystallin domain, the second Greek key motif is floppy as compared to its relatively rigid counterpart. Taken together, we believe that these characteristics might be of importance to understand the stability and functions of βγ-crystallin domains.

1. Introduction

The protein structures determined by NMR and X-ray Crystallography are static, and correspond to the lowest energy or ground-state conformation. The function of a protein depends on its brief excursions to the slightly higher energy conformations [1–3]. These excursions are possible due to the conformational flexibility associated with the structure. The protein molecules are dynamic entities and have fast fluctuations of small amplitude about their equilibrium/native structure. However, sometimes these fluctuations become large enough to result in the less frequent deformations, which may finally give rise to states that can be defined as 'alternative states' of slightly higher energy than that of the ground state. These alternative states are populated to a very small extent because of the highly cooperative nature of protein folding and are hence difficult to study. However, NMR spectroscopy plays an important role in this respect to probe these fluctuations in solution state, as they influence various relaxation mechanisms and thereby provide the details of the involved molecular motions/dynamics. A better understanding of native and near native alternative states together with the knowledge of motions at various timescales present in the molecule is indispensable as several proteins have been shown to function by occupying these excited states [4].

The βγ-crystallin superfamily consists of members that belong to various taxa that range from archea to vertebrates. Most of them are structural proteins with high intrinsic stability, which further gets enhanced upon addition of Ca^{2+}, particularly in the case of microbial members [5]. The functions of most of the members of this superfamily are yet to be known; though a few of them have been reported to be involved in Ca^{2+}-dependent stress related functions [6]. Since then there have been attempts to understand their Ca^{2+}-binding properties and biological function. To date, there is only one report on the equilibrium dynamics of a βγ-crystallin domain [7], perhaps because these domains are known to be structural proteins with unknown functions. Further, the dynamics of other Ca^{2+}-binding domains, for instance EF-hand domains, are better understood. Therefore, we set out to study the equilibrium dynamics at different timescales and the presence of low-lying free-energy states in native and near-native conditions of a microbial homolog of βγ-crystallin, hahellin, using NMR spectroscopy [8]. Hahellin is a natively unfolded protein that acquires a well-folded structure upon Ca^{2+} binding. The study of its dynamics in the Ca^{2+}-bound form will be crucial to understand the characteristics of the βγ-crystallin domains.

Abbreviations: DSC, Differential Scanning Calorimetry; TOCSY, TOtal Correlation SpectroscopY; NOESY, Nuclear Overhauser Effect SpectroscopY; HSQC, Heteronuclear Single Quantum Correlation; HMQC, Heteronuclear Multiple Quantum Correlation; SOFAST, band-Selective Optimized-Flip-Angle Short-Transient; NOE, Nuclear Overhauser Effect; DSS, 4,4-dimethyl-4-silapentane-1-sulfonic acid; CARA, Computer Aided Resonance Assignment; BMRB, Biological Magnetic Resonance Data Bank; TATAPRO, Tracked Automated Assignments in PROteins; RMSD, Root Mean Square Deviation.

* Corresponding author at: 1-Homi Bhabha Road, Navy Nagar, Colaba, Mumbai-400005, India. Tel.: +91 22 2278 2489; fax: +91 22 2280 4610.
E-mail addresses: atulks@tifr.res.in (A.K. Srivastava), chary@tifr.res.in (K.V.R. Chary).
[1] D-220A, Department of Chemical Sciences, Tata Institute of Fundamental Research, 1-Homi Bhabha Road, Navy Nagar, Colaba, Mumbai-400005, India. Tel.: +91 022 2278 2271; fax: +91 22 2280 4610.

0301-4622/$ – see front matter © 2011 Elsevier B.V. All rights reserved.
doi:10.1016/j.bpc.2011.04.001

2. Materials and methods

2.1. Protein expression and purification

Hahellin was overexpressed and purified as described elsewhere [9]. Uniformly $^{13}C/^{15}N$-labeled protein samples were produced in an isotopically labeled M9 minimal medium containing 1 g/l $^{15}NH_4Cl$ with or without 4 g/l ^{13}C-glucose as the sole nitrogen and/or carbon source, respectively. The protein overexpressed in the form of inclusion bodies, which were subjected to denaturation and then the protein refolding was carried out using ion-exchange chromatography as described earlier. Size exclusion chromatography was performed as the final purification step. The sample was prepared in a buffer solution of 10 mM Tris·Cl, 300 mM NaCl, and 20 mM $CaCl_2$ at pH 6.7.

2.2. Differential scanning colorimetry

The thermal denaturation of hahellin was studied by differential scanning calorimetry (DSC) using VP-DSC Microcalorimeter (MicroCal LLC). The protein concentration was 237 μM. The temperature of the protein sample was increased from 10 to 80 °C (scan-up) and then decreased back to 10 °C (scan-down) with a scan rate of 1 degree/min. The scans were repeated to check the reversibility of the thermal denaturation process. Baseline correction was done by recording buffer solution under similar experimental conditions and then subtracting it from that of the protein. The variation in the molar heat capacity of hahellin with temperature was monitored. The curves thus obtained were fitted with different models of thermal unfolding (see the Supplementary material-1).

2.3. NMR spectroscopy

The ^1H, ^{13}C and ^{15}N resonances of almost all the backbone nuclei were assigned earlier using a standard suite of three-dimensional (3D) NMR experiments, namely, ^{15}N-edited TOCSY and NOESY, HNCA, HN(CO)CA, HNCO, HN(CA)CO, CBCA(CO)NH, CBCANH. The assigned chemical shifts have been deposited in the BioMagResBank (http://www.bmrb.wisc.edu) under the accession number 15743 [10].

The sample for NMR spectroscopy was prepared by concentrating the protein solution in a buffer (10 mM Tris.Cl, 300 mM NaCl, 20 mM $CaCl_2$, pH 6.75), with a volume of 540 μl. Later, 40 μl of ^2H_2O was added for field locking purpose. The concentration of the protein was estimated to be ~0.8 mM. The proton chemical shifts were referenced using DSS (2,2-dimethy-2-silapentane-5-sulphonate), as an external reference, at 0.0 ppm. The ^{15}N chemical shift was referenced indirectly. All NMR experiments were carried out at 25 °C on Bruker Avance 800 MHz equipped with a pulsed-field gradient unit and a triple-resonance cryo-probe that has actively shielded Z-gradients. NMR data processing was done using Felix 2002 (Accelrys Inc., Sandiego) and spectral assignment was achieved using TATAPRO [11] and CARA (http://cara.nmr.ch/doku.php). The temperature of the NMR probe was calibrated using chemical shift differences of proton resonances as observed in methanol (280 to 300 K) and ethylene glycol (300 to 320 K) samples [12].

A set of 2D ^1H-^{15}N HET-SOFAST-HMQC experiments [13] was recorded with a contact time (t_c) of 200 ms. Selective ^1H inversion pulses were applied on water resonance and at the center of aliphatic protons for the HET^{ex}- and HET^{noe}-SOFAST experiments, respectively.

The pulse sequences for the measurement of the longitudinal (T_1) and transverse (T_2) relaxation times and the $\{^1H\}$-^{15}N heteronuclear NOE of the backbone ^{15}N nuclei have been described previously [14]. The transverse relaxation rates (R_2) were measured with relaxation delays of 23.36, 46.72, 70.08, 93.44, 116.8, 140.16, 163.52 and 186.88 ms. The CPMG delay ($2\,\tau_{cp}$) was set to 1.3 ms. The longitudinal relaxation rates (R_1) were measured with relaxation delays of 10, 50, 100, 200, 400, 600, 800 and 1000 ms. Certain duplicate spectra were recorded for the estimation of errors in the measured intensities. An interleaved 2D $\{^1H\}$-^{15}N NOE experiment was recorded with a 4 s recycle delay. The spectral widths were 11 and 26 ppm along ^1H and ^{15}N dimensions, respectively. The spectra were acquired with 128 and 1024 complex points along indirect and direct dimensions, respectively, and processed with 1024 and 4096 points using a 60° shifted sine-square-bell window function.

The reduced spectral density functions, $J(0)$, $J(\omega_N)$ and $J(0.87\omega_H)$ were calculated using ^{15}N chemical shift anisotropy ($\Delta\sigma$) as −163 ppm and average N—H bond length as 1.02 Å, at a magnetic field of 18.8 T. The correlations between $J(0)$ with $J(\omega_N)$ and $J(0.87\omega_H)$ were simulated using Mathematica 7.0, with the assumption of completely rigid molecule tumbling at ω_N and ω_H angular frequencies.

The temperature dependence of amide proton ($^1H^N$) chemical shifts was monitored by recording [^{15}N-^1H]-HSQC spectra at temperatures ranging from 280 to 313 K with a constant interval of 3 K. Thereafter, the temperature was reduced to 298 K to check the reversibility and the stability of the sample by comparing its HSQC spectra. The same experiment was performed at denaturing concentrations of 0.3, 0.6 and 0.9 M urea. All the spectra were referenced using DSS as an external reference at 298 K and then adding the correction of 0.01 ppm/K for the temperature change [15]. The peaks in the HSQC at 298 K were assigned as described earlier [10]. The spectra at other temperatures were assigned by visual inspection as the changes in chemical shifts were small and unambiguous (see the Supplementary Figures S1 and S2).

2.4. Determination of spectral density functions, tumbling time and $\lambda_{noe/ex}$

The R_1, R_2 and $\{^1H\}$-^{15}NOE ratios were measured for 87 of 92 residues present in hahellin; the first three residues (Met1, Gly2 and Glu3) could not be assigned. Hence, these and two Pro residues (P22 and P47) could not be used in measuring the relaxation parameters associated with them.

The spectral peak intensities (heights) for the determination of relaxation parameters T_1 and T_2 were determined as a function of time using Felix software (Accelrys, 2002) and fitted as single exponential decays with the help of a Mathematica program (http://www.wolfram.com/). The error in the peak intensity was estimated as the root mean square deviation of peak to peak intensity using duplicate spectra. The $\{^1H\}$-^{15}N NOE was calculated as the ratio of the peak intensities in the spectra recorded with and without ^1H saturation. The error was estimated as root mean square deviation of the noise in the spectra.

The spectral density functions at zero Larmor frequency ($J(0)$), and at Larmor frequency of ^{15}N ($J(\omega_N)$) and ^1H ($J(\omega_H)$) were obtained using equations [16] as described in the Supplementary material-2.

The $J(\omega_N)$ values thus obtained were plotted against $J(0)$ and fitted with an empirical linear equation, $J(\omega_{N,H}) = \alpha\ J(0) + \beta$, to obtain the associated intercept (β) and slope (α). The correlation times were obtained using the equation [17]: $2\alpha\,\omega_N^2\tau_m^3 + 5\beta\,\omega_N^2\tau_m^2 + 2(\alpha-1)\tau_m^3 + 5\beta = 0$; here, τ_m and ω_N are correlation time and ^{15}N frequency, respectively.

The $\lambda_{noe/ex}$ values were obtained as a ratio of peak intensities in the spectra recorded with (I_{sat}) and without inversion (I_{ref}) of aliphatic or water proton resonances, using $HET^{noe/ex}$-SOFAST experiments.

2.5. Determination of curved temperature dependence of $^1H^N$ chemical shifts

All the peaks in the spectra were picked manually and the chemical shifts were collected for each temperature point. For each residue, the $^1H^N$ chemical shifts were plotted as a function of temperature and were fitted to a straight line. The deviations from the straight line (the residuals) were then determined and plotted

against temperature, and were examined visually to observe the curvature. Data analysis was done using SigmaPlot (version 11.0) and a home-built Mathematica program.

The theoretical curves for the temperature dependence of $^1H^N$ chemical shifts were simulated for the temperature ranging from 280 to 313 K, using Mathematica (Version 7.0) and the figures were generated using SigmaPlot (Version 11.0). Further details are given in the figure legends.

3. Theory of curved temperature dependence of $^1H^N$ chemical shifts

The theory of the non-linear temperature dependence of $^1H^N$ chemical shift is as follows [18,19]. The protein is assumed to exist in two equilibrium conformations, which are in fast exchange on the chemical shift timescale. Thus, the observed chemical shift would be the population weighted average of the chemical shifts corresponding to the two states,

$$\delta_{obs} = \delta_1 p_1 + \delta_2 p_2 \tag{1}$$

where,

$$\delta_1 = \delta_1^0 p_1 + g_1 T \tag{2a}$$

$$\delta_2 = \delta_2^0 p_2 + g_2 T \tag{2b}$$

and δ_n is the chemical shift, g_n is the gradient of temperature dependence and p_n is the fractional population of conformation n. The two states have been assumed to be separated by a free energy difference ΔG given by

$$\Delta G = \Delta H - T\,\Delta S. \tag{3}$$

The ΔH (enthalpy difference) and ΔS (entropy difference) have been assumed to be independent of temperature. The populations of the two conformations are related by,

$$\frac{p_2}{p_1} = e^{-\Delta G/RT} \tag{4}$$

where R is the universal gas constant and T is the absolute temperature.

Therefore, the observed chemical shift is given by

$$\delta_{obs} = \frac{\left(\delta_1^0 + g_1 T\right) + \left(\delta_2^0 + g_2 T\right) e^{-\Delta G/RT}}{1 + e^{-\Delta G/RT}}. \tag{5}$$

This model explains the curved temperature dependence of an $^1H^N$ chemical shift (see Supplementary material-3). To understand the effect of ΔG, δ_n^0, g_n etc., we have simulated the behavior of $^1H^N$ chemical shift within the temperature range of 275–315 K using Eq. (5).

The δ_{obs} values simulated as a function of temperature were fitted to a straight line, and the residuals were determined and plotted against temperature to produce the profiles of the deviations.

4. Results and discussion

4.1. Thermodynamic stability

The thermodynamic stability of hahellin was determined by DSC. The variation of molar heat capacity with temperature results in a sharp symmetrical bell shaped curve, which is a characteristic of the cooperative two-state thermal unfolding (Fig. 1). The curve fitting with the two-state model resulted in a calorimetric enthalpy of 83.93 kcal/mol and melting temperature as 51 °C. The van't Hoff enthalpy was obtained as 89.43 kcal/mol by fitting the DSC curve with a non-two-state model (see Supplementary material-1). The close similarity of calorimetric enthalpy values to that of the van't Hoff enthalpy confirms that the thermal unfolding of hahellin is indeed a two-state cooperative process. Further, the ΔC_p was determined by the DSC curve without baseline correction and fitting it with the two-state model with ΔC_p effects. A positive ΔC_p (909 ± 36 cal mol^{-1} °C^{-1}) is expected as the protein unfolds on increase in the temperature. The values of various thermodynamic parameters thus obtained are listed in Table 1.

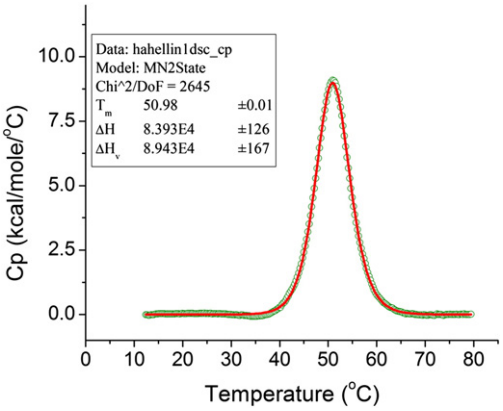

Fig. 1. DSC thermogram observed for unfolding of Ca^{2+}-bound hahellin. The experimental data points are shown by green circles and the best fit by the solid red line. The fitting was done with non-two-state model.

These thermodynamic parameters were incorporated into Gibbs–Helmholtz equation to give the value of $\Delta G_{unfolding} = 5.87$ kcal/mol. This indicates that hahellin is marginally stable. Further, the melting transition spans the temperature range of 40–60 °C with the melting temperature as 51 °C. It shows that hahellin stays in the folded globular native state ensemble below 40 °C. This allowed us to vary the temperature of the protein from 7 to 40 °C to investigate the low lying free energy states without causing any unfolding.

4.2. Curved temperature dependence of $^1H^N$ chemical shifts

The presence of curvature in $^1H^N$ chemical shifts as a function of temperature, which is otherwise linear, is an evidence of the presence of more than one (here two) states exchanging with each other with a fast rate on the chemical shift timescale. The effects of chemical shifts (δ_n^0) and temperature gradients (g_n) of protein molecules belonging to these states on the behavior of the temperature dependence of $^1H^N$ chemical shifts were explored by simulating the curves. The simulated curves are shown in Fig. 2. For all simulations, δ_1 and δ_2 were set to 8.5 and 8.0 ppm, respectively, and gradients g_1 and g_2 were set to −2.0 and −7.0 ppb/K respectively. In all the simulations, the observed chemical shifts were calculated and then fitted to a straight line, and then the residuals were plotted against temperature as mentioned earlier. The lower value of δ_2

Table 1
The thermodynamic parameters obtained by fitting the DSC curves to various models. ΔH_{cal} is the calorimetric heat and $\Delta H_{van't}$ is van't Hoff enthalpy. T_m is the melting temperature of the protein.

Fitting model	T_m (°C)	ΔH_{cal} (cal mol^{-1})	$\Delta H_{van't}$ (cal mol^{-1})	ΔC_p (cal mol^{-1} °C^{-1})
Two state	50.98 ± 0.01	$8.63E4 \pm 103$		
Non-two state	50.98 ± 0.01	$8.40E4 \pm 126$	$8.94E4 \pm 167$	
Two state, C_p	50.77 ± 0.02	$8.73E4 \pm 96$		909 ± 36

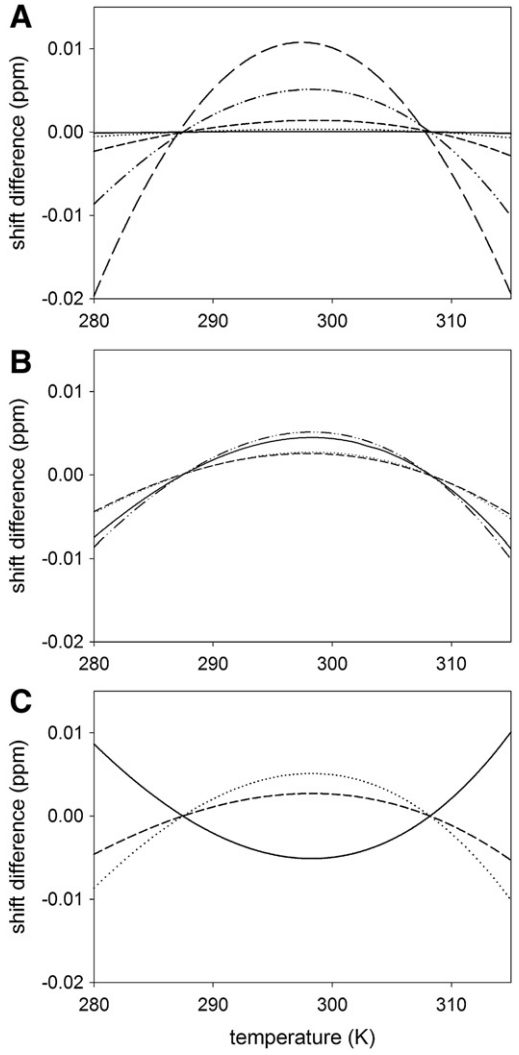

Fig. 2. (A) Simulations of the dependence of H^N chemical shift variations with temperature on difference in free energy between ground and excited states. The calculation was done using enthalpy difference of 6.1 (big dash), 7.1 (dot–dot dash), 8.1 (dash), 9.1 (dotted) and 10.1 (solid line) kcal/mol, corresponding to free energy difference at 298 K of 1, 2, 3, 4 and 5 kcal/mol, respectively. The $T\Delta S$ was taken as 5.1 kcal/mol at 298 K. (B) Simulation of the dependence of H^N chemical shift variation with temperature on the features of excited states. The curve (dot–dot dash) is the same as in Fig. 2A, for $\Delta G = 2$ kcal/mol. The other curves show a state with more similar chemical shift to ground state (solid: $\delta_2 = 8.3$ ppm); more similar gradients (dotted: $g_2 = -4$ ppb/K) and more similar entropy (dashed: $\Delta S = 10.2$ cal/molT^{-1} and $\Delta H = 5$ kcal/mol, leaving ΔG still at 2 kcal/mol). (C) Simulation of the dependence of H^N chemical shift variation with temperature. The dotted curve is the same as in Fig. 2A, for $\Delta G = 2$ kcal/mol. The solid (concave) curve shows the behavior when excited state characteristics exchanged with ground state. That is $\delta_1^0 = 8.0$ ppm, $\delta_2^0 = 8.5$ ppm, and gradients $g_1 = -7.0$ ppb/K and $g_2 = -2.0$ ppb/K. The change in free energy and change in entropy have been kept same, that is $\Delta G = 2$ kcal/mol and $\Delta S = 17.2$ cal mol^{-1} K^{-1} at 298 K.

compared to δ_1 is justified as the protein is predominantly in a rigid β-sheet conformation (δ_1) and is expected to transform into a random-coil conformation (δ_2) upon increase in the temperature. Further, the g_1 and g_2 values were set to −2.0 and $g_2 = -7.0$ ppb/K as they were experimentally determined as average values corresponding to the rigid β-strand and the flexible (C-terminal tail) parts of the protein, respectively (see Fig. 4).

A simple observation of the simulation reveals that the curvature decreases with the increase in ΔG and starts vanishing at $\Delta G = 4$ kcal/mol in the temperature range of 280–313 K, keeping other parameters constant (Fig. 2A). The curvature also decreases with the decrease in the difference of the chemical shifts or temperature gradients of the two conformational states or the decrease in the entropy change ΔS, keeping ΔG constant (Fig. 2B). The nature of the curve is convex (positive curvature) when the chemical shift of the ground state is more down field shifted as compared to that of an excited state; the concave curve is observed in the reverse situation (Fig. 2C). Based on these results one can conclude that the absence of the curvature does not guarantee the absence of alternative conformational state(s), however, it does put some limits on ΔG values required for the observation of the non-linear behavior.

4.3. The low lying alternative states

The marginal stability is an essential quality of proteins as it allows the access of slightly higher energy states which might correspond to distinctly different conformations from the ground state, and might be crucial for the biological functions.

Although it is still very difficult to map the whole folding funnel for a protein, such investigations on the low lying free energy states may throw some light on the free energy landscape at the bottom of the folding funnel, where most of the protein functions are played. Therefore, we set out to look into such low lying alternative states by the method of *non-linear temperature dependence* of $^1H^N$ chemical shifts, in native and near-native conditions generated by a mild urea denaturation of the protein.

The presence of non-linear temperature dependence along the protein sequence indicates that the associated residues access some alternative conformations (Fig. 3). In the present study, all such residues are distributed along the protein sequence and are as follows: V6, L8, Y9, D11, H13, K15, Y17, V19, V23, G24, I32, N38, D40, L41, G49, E53, Q56, H57, N58, D65, T68, S69, L74, S75, R76, D77, A80, S81, S86 and K87. Some of these residues are at the edges of β-strands and α-helix. Residues such as Y9, D11, H13 N38, D40, and L41 belong to the Ca^{2+}-binding loop of the first Greek key motif, while Q56, H57, N58, L74, S75, R76, and D77 belong to the Ca^{2+}-binding loop of the second Greek key motif. Residues V23 and G24 are part of a local structural motif called *Tyr corner*, which consists of a Tyr residue that interacts with the preceding residue G24. All these positions in the protein are associated with loose local structures which are bestowed with the scope of some flexibility. All the curvatures are positive and describe a situation where the excited state chemical shift is up-field shifted as compared to that of the ground state.

It may be noted here that residues D11, T12, K15 and Y17 (~0.5 ppb/K), N78 and A80 (~1.6 ppb/K) and L41 (3.87 ppb/K) show positive temperature coefficients (Fig. 4). Usually, the temperature coefficients of $^1H^N$ chemical shifts are negative due to the increase in the hydrogen-bond lengths caused by thermal perturbations. However, the complex architecture of the protein does allow an exception to this rule due to subtle changes in the microenvironment favorable for the positive temperature coefficient; for example D11, T12, K15 and Y17 might be affected by the ring currents of nearby situated aromatic residues such as Y9, F14 and Y17 (Fig. 5). But L41, N78 and A80 do not have any agency causing such effects. Interestingly, these residues belong to the Ca^{2+}-binding loops, where there is a possibility of accessing the alternative conformations, which in this case might be associated with downfield shifted chemical shifts.

Further, the above mentioned temperature dependence experiments were carried out at increasing concentrations of urea, namely, 0.3, 0.6 and 0.9 M, under identical experimental conditions, to allow more residues to access the alternative states by loosening the protein scaffold. Interestingly, no apparent spectral changes were observed (See Supplementary Figure S3). Comparing the experimentally observed curvatures obtained at various sub-denaturing conditions, with those of the simulated ones, we found that the alternative states lie within ~2 kcal/mol free energy difference from the ground state. This difference is found to be smaller (~1 kcal/mol) where the curvature is stronger. The conformations belonging to these states are

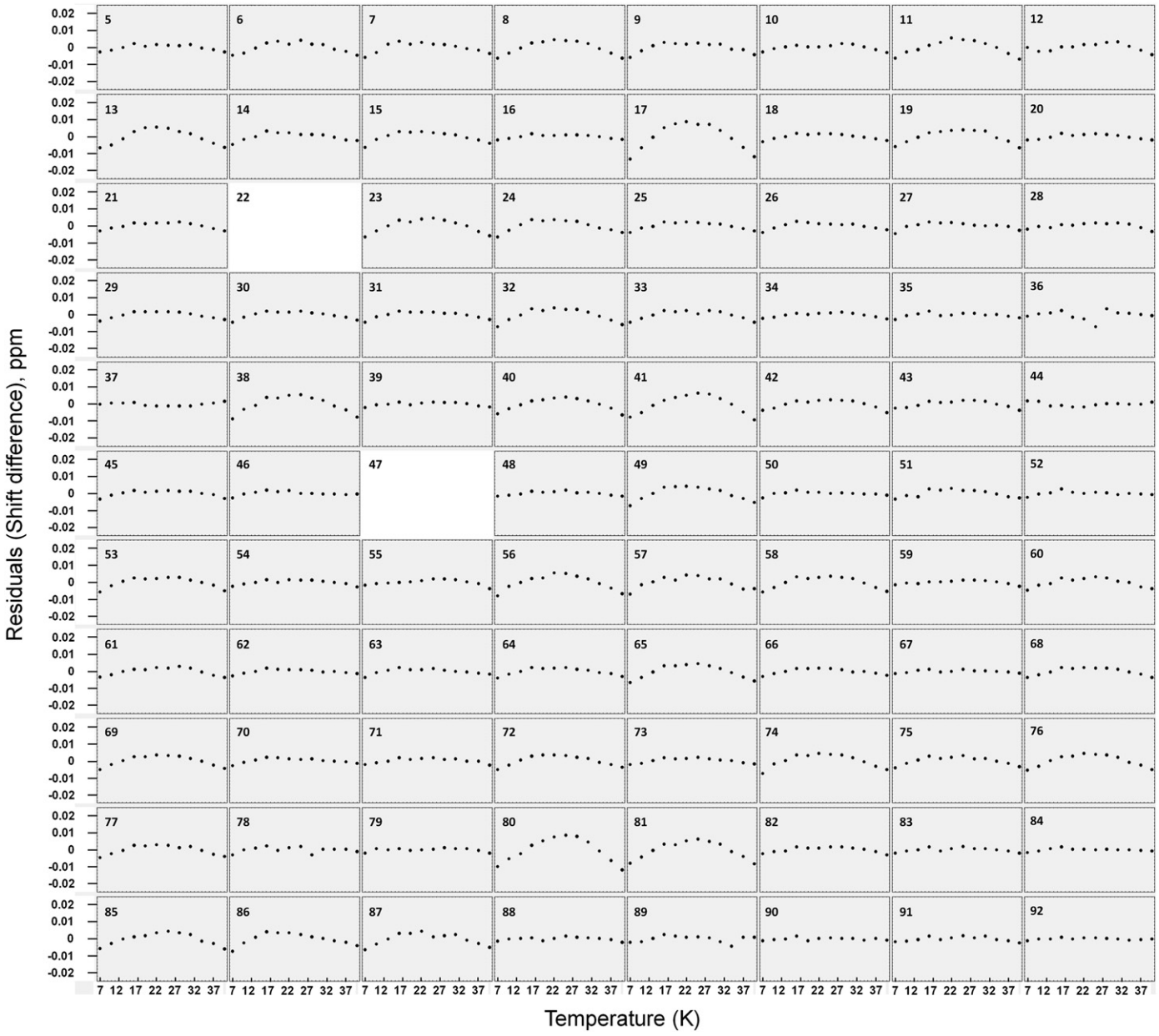

Fig. 3. Residuals obtained after fitting the straight line to the variation of amide proton chemical shift with respect to temperature. The number shown within the boxes denotes the number of amino acid residue in the sequence. The two empty boxes correspond to P22 and P47. The vertical scale spans 0.05 ppm and the horizontal scale as 33 K of temperature range.

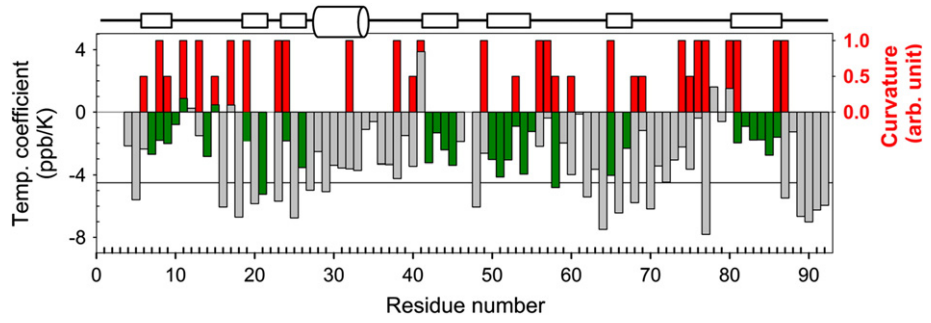

Fig. 4. The temperature coefficients of amide proton chemical shift are plotted against residue number. The magnitude of gray and green bars corresponds to the value of temperature coefficient; the bars corresponding to amide protons which remain even after 12 h after deuterium exchange are green colored. The horizontal black line taken as cutoff (4.5 ppb/K) for amide protons involved in hydrogen bonding. The red bars indicate the residues that showed curved temperature dependence; the height of the bar corresponds to strong (1.0) and mild curvature (0.5) in arbitrary unit, and was determined by visual examination of the curvatures. The location of secondary structure elements along the sequence is shown by rectangular box (β-strand) and a cylinder (α-helix) on top of the plot.

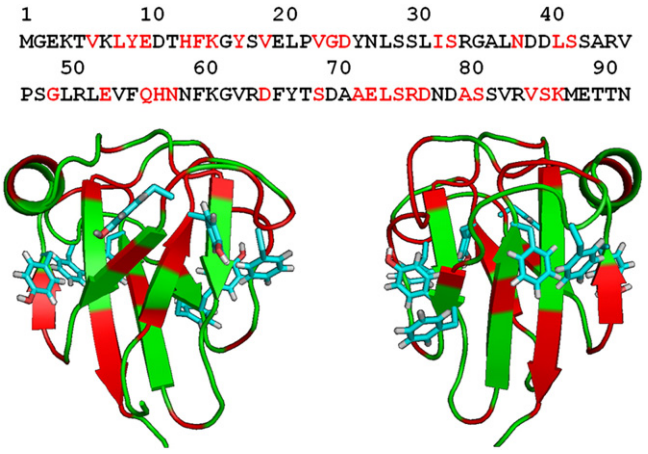

Fig. 5. The presence of curvatures, obtained from the temperature dependence of amide proton chemical shift, is indicated in the sequence by red colored one letter amino acid code. These locations of these residues are mapped on structure (ribbon diagram) of hahellin and are indicated by red color. The aromatic side chains are depicted in cyan color.

in a fast exchange at the chemical shift timescale as each residue shows only a single peak in HSQC.

The NMR timescale for ^{1}H resonances at 800 MHz spectrometer, is about 400 s^{-1} (taking chemical shift difference of 0.5 ppm, as the same difference was used in the simulation), which implies that the rate of interconversion between these conformations would be at least 400 s^{-1}. Considering it as a minimum of the rate constant, k, for such exchange reaction, the maximum possible activation free energy barrier could be estimated as 3.44 kcal/mol using $\Delta G \cong -RT \ln k$, at 298 K. The fact, that the chosen sub-denaturing (or near-native) conditions do not affect the observation made in the native state, reveals that the free-energy landscape is not malleable.

4.4. Conformational dynamics

The intramolecular motions associated with a macromolecule at various frequencies can be described in terms of spectral density functions, which can be calculated from experimentally derived relaxation parameters. There are two techniques commonly used for such investigations; Model Free approach and Spectral Density Mapping. We have used reduced spectral density mapping because it is easier to perform and does not involve any model per se.

In *reduced spectral density mapping*, the spectral density functions, $J(0)$, $J(\omega_N)$, and $J(0.87\omega_H)$ are calculated from relaxation parameters, R_1, R_2 and $\{^{1}H\}$-^{15}NOE.

The slope (α, 0.038) and intercept (β, 0.207 rad nsec^{-1}) were obtained for the best fit to the plot of $J(\omega_N)$ against $J(0)$; ω_N is 5.098×10^{8} rad sec^{-1}. The cubic equation produced three roots (correlation time, τ_m); −189.00, 0.59 and 4.71 nsec rad^{-1}. We assigned tumbling time for hahellin as 4.71 nsec rad^{-1}, which is expected for 10 kDa globular protein. This shows that hahellin exists

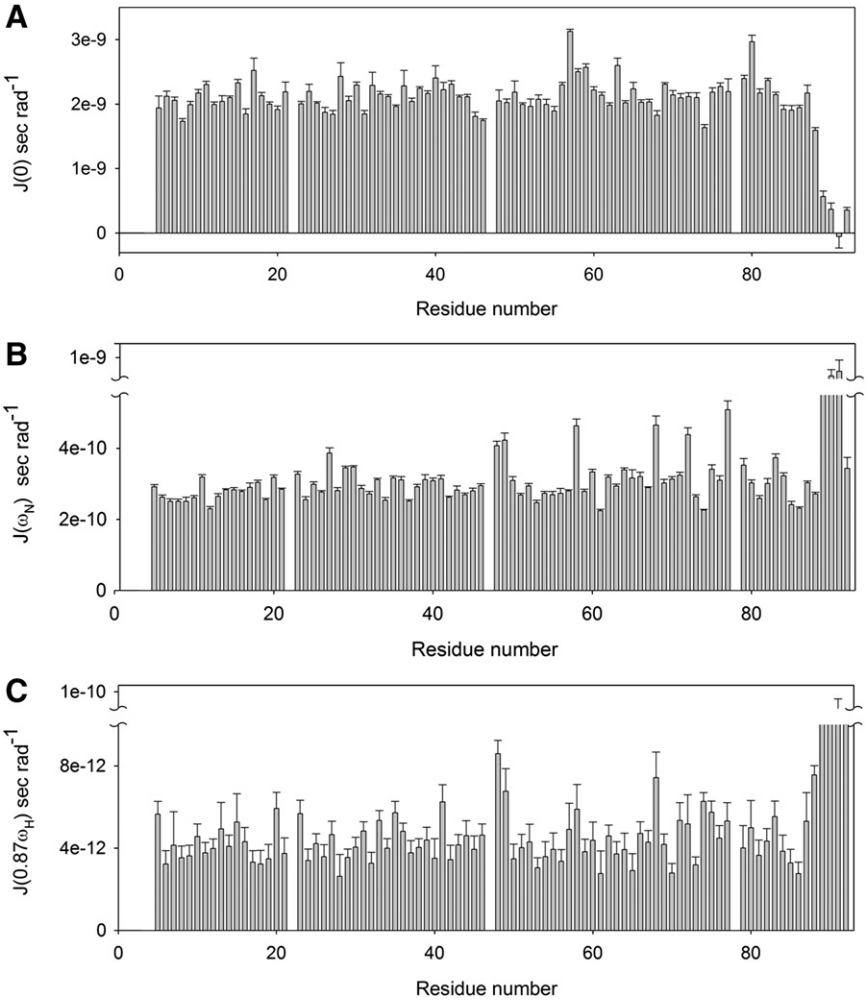

Fig. 6. Reduced spectral density functions at (A) zero frequency (J(0)), and at frequency of (B) ^{15}N ($J(\omega_N)$) and (C) ^{1}H ($J(\omega_H)$) nuclei, are shown by bars and plotted against the residue number. The associated errors are shown on the top of each bar.

as a monomer even at higher concentrations. The second root, that is 0.59, is possibly the correlation time for faster internal motion.

The value of $J(0)$ is sensitive to the very slow motions whereas $J(\omega_N)$, and $J(0.87\omega_H)$ are sensitive to the relatively faster motions at ω_N and ω_H frequencies, respectively (Fig. 6). The plots of $J(0)$ against $J(\omega_N)$ (Fig. 7A) and that against $J(\omega_H)$ (Fig. 7B) show clustering of the amino acid residues in the specific regions. Such type of plot can be used for qualitative analysis of the spectral density functions. Here, the red curve (Fig. 7) is obtained as follows: for isotropic rotor the spectral density (J(ω)) is given as,

$$J(\omega) = \frac{2}{5}\frac{\tau}{1 + (\omega\ \tau)^2}. \quad (6)$$

If the dynamics is limited to a single motion, one can write

$$J(0) = \frac{2}{5}\tau \quad or \quad \tau = \frac{5}{2}J(0). \quad (7)$$

Putting τ equal to $2.5 \times J(0)$, one can obtain a relation between J(0) with $J(\omega_N)$ and $J(\omega_H)$ as given below:

$$J(\omega_N) = \frac{J(0)}{1 + 6.25(\omega_N\ J(0))^2} \quad (8)$$

and

$$J(\omega_H) = \frac{J(0)}{1 + 6.25(\omega_H\ J(0))^2}. \quad (9)$$

This is the basis for the simulated red curve shown in Fig. 7A and B. Most of the residues fall in the regions described by the simulated curves (Eq. 8 and 9) and therefore are described as ones with restricted N—H bond motion relative to the overall tumbling of the molecule [20]. However, there are some distinct deviations. The residues E89, T90 and N92 lie in the region of extremely low $J(0)$ and high $J(\omega_N)/J(\omega_H)$ and therefore they are found to be highly flexible. Residue T91 is located in the same region but with a slightly negative $J(0)$ value, and therefore it is not shown in Fig. 7. These residues belong to the C-terminal end of the protein. The residues A80 and H57 belong to the very low $J(\omega_N)/J(\omega_H)$ and high $J(0)$ values, showing relatively slow motion and might be involved in a conformational exchange. Besides these, there are other residues showing conformational exchange and can be more clearly seen in the $J(0)$ versus $J(\omega_N)$ plot. These include D77 and N58 and also N27, S48, G49, N68, A72 and D79. Except N27, the residues involved in μs–ms timescale motions belong to the second half of the protein sequence that consists of C-terminal Greek key motif. It indicates that this part is relatively less rigid and has a tendency to adopt a floppy conformation to facilitate such motions. In contrast, the first half of the protein sequence (N-terminal Greek key motif) does not show such signatures. The heteronuclear $\{^1H\}$-^{15}N NOE (See Supplementary Figure S4) reveals that all the amide protons are sufficiently rigid with respect to the molecule. All this indicates a synchronized segmental motion of the second Greek key motif. This prompted us to explore the compactness and the structural heterogeneity along the protein sequence using a set of 2D ^1H—^{15}N HET-SOFAST-HMQC experiments, as described below.

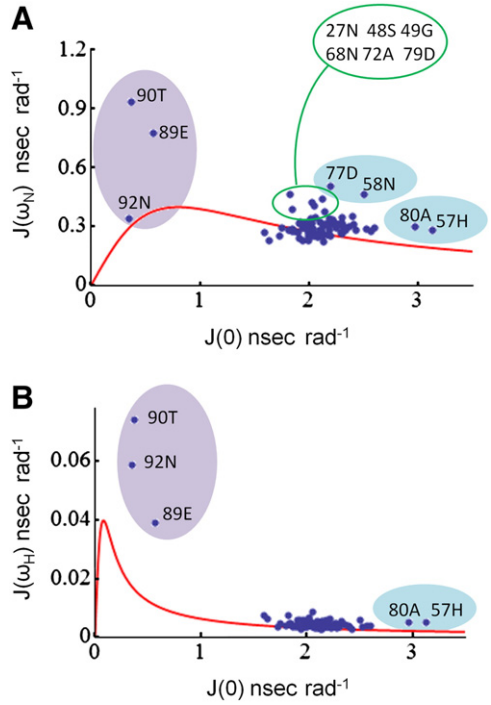

Fig. 7. Correlation plot obtained by plotting (A) $J(\omega_N)$ and (B) $(J(\omega_H))$ against $J(0)$ The simulated correlation is represented by the red thick line. The regions of fast and slow motions are shown by light purple and cyan colors, respectively. Each blue dot represents the location of amino acid residue on the plot; the relevant ones are assigned with residue number followed by one letter code.

4.5. Compactness and conformational heterogeneity

A parameter λ (I^{sat}/I^{ref}) is derived from the ratio of the peak intensities obtained in a reference spectrum (no inversion) to those obtained when a selective pulse inverts the water (HET^{ex}-SOFAST) or the aliphatic resonances (In HET^{noe}-SOFAST) of the protein. The inverted aliphatic resonances reduce the intensities of N—H cross peaks by spin-diffusion/NOE effect as they relax towards the equilibrium. Similarly, the inverted water resonances lower the N—H cross peaks intensities through exchange of amide protons with that of the solvent (water). The measures of spin-diffusion/NOE and amide–water exchange are λ^{noe} and λ^{ex}, respectively. The compact structure will have λ^{noe} less than 1 but $\lambda^{ex} \approx 1$; however the open or less compact structure will exhibit $\lambda^{noe} \approx 1$ but λ^{ex} less than 1 [13]. Thus, these values provide complementary information about the structural heterogeneity and the local compactness of the protein structure. The residues belonging to the first Greek key of hahellin are characterized by an average value of λ^{noe} ~0.1 and the λ^{ex} ~0.7 in the regions of defined secondary structure elements; the loops show relatively lower λ^{ex} and higher λ^{noe} (Fig. 8A). However, the residues belonging to the second Greek key motif show λ^{noe} ~0.2–0.5 and λ^{ex} ~0.2–0.6, except at the C-terminal end where they possess $\lambda^{noe} \approx 0.9$ and $\lambda^{ex} \approx 0.1$. Based on these results we demonstrate that the second Greek key motif possess a fair amount of plasticity (Fig. 8B, C).

5. Conclusion

We have studied the motional dynamics in hahellin, a βγ-crystallin domain, at residue level. Hahellin is shown to possess large structural heterogeneity as nearly 40% of amino acid residues access alternative states, even in the native state ensemble. These alternative states are accessed with conversion rates of at least 400 Hz and are separated from the ground state by an activation free energy of 3.44 kcal/mol. Most of the residues show linear temperature coefficient with a negative slope, while a few show positive temperature coefficients. The latter might arise due to the complex protein architecture. We attempted to increase the number of residues accessing these alternative states by slightly altering the protein scaffold using chemical denaturation (0.3 to 0.9 M urea). The mild denaturation maintained the native state ensemble, and did not affect the curvatures. This shows that the free energy landscape at the

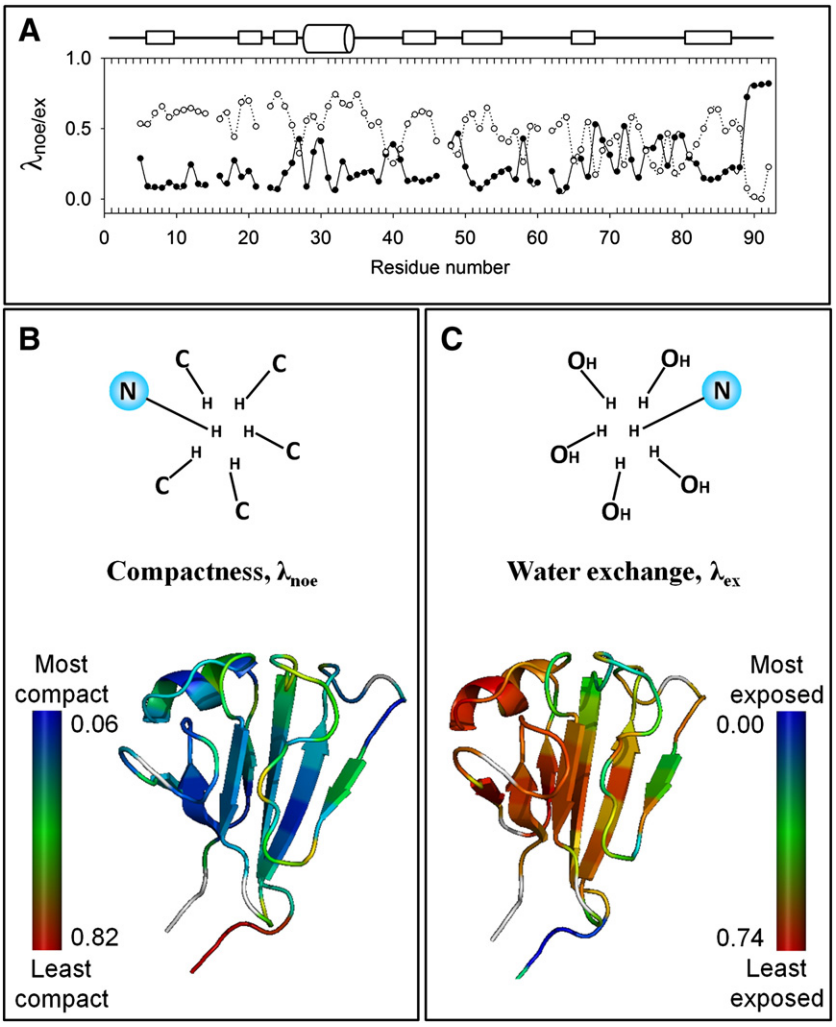

Fig. 8. Structural heterogeneity in hahellin: (A) λ_{noe} (filled circle) and λ_{ex} (open circle) are plotted against residue number. The location of secondary structure elements along the sequence is shown by rectangular box (β-strand) and a cylinder (α-helix) on top of the plot. The values of λ_{noe} (B) and λ_{ex} (C) are mapped on hahellin's structure (ribbon diagram) with color coding defined by the color bars. The white color is used for proline residues.

bottom of the folding funnel is sufficiently robust against such perturbations.

We also observed the residues involved in slow motions (μs–ms) that belong to the second Greek key motif of hahellin, making it relatively more floppy. A similar type of observation (using B-factor) is made (data not shown) in Protein S that has the closest match in structure with hahellin (RMSD, 1.3). Thus, this study is an attempt to understand the dynamical features of such domains and might be crucial for the understanding of stability and function in the βγ-crystallin superfamily.

Supplementary materials related to this article can be found online at doi:10.1016/j.bpc.2011.04.001.

Acknowledgments

The facilities provided by the National Facility for High Field NMR, and the support of the Department of Science and Technology (DST), Department of Biotechnology (DBT), Council of Scientific and Industrial Research (CSIR), and Tata Institute of Fundamental Research (TIFR), Mumbai, are greatly acknowledged. We thank Mr. Dinesh Kumar for his help in the SOFAST-HMQC experiments and in Mathematica.

References

[1] F.A. Mulder, A. Mittermaier, B. Hon, F.W. Dahlquist, L.E. Kay, Studying excited states of proteins by NMR spectroscopy, Nat. Struct. Biol. 8 (2001) 932–935.
[2] F.A. Mulder, B. Hon, A. Mittermaier, F.W. Dahlquist, L.E. Kay, Slow internal dynamics in proteins: application of NMR relaxation dispersion spectroscopy to methyl groups in a cavity mutant of T4 lysozyme, J. Am. Chem. Soc. 124 (2002) 1443–1451.
[3] L.E. Kay, Protein dynamics from NMR, Nat. Struct. Biol. 5 Suppl (1998) 513–517.
[4] A.J. Baldwin, L.E. Kay, NMR spectroscopy brings invisible protein states into focus, Nat. Chem. Biol. 5 (2009) 808–814.
[5] R. Jaenicke, C. Slingsby, Lens crystallins and their microbial homologs: structure, stability, and function, Crit. Rev. Biochem. Mol. Biol. 36 (2001) 435–499.
[6] G. Wistow, L. Summers, T. Blundell, Myxococcus xanthus spore coat protein S may have a similar structure to vertebrate lens beta gamma-crystallins, Nature 315 (1985) 771–773.
[7] R. Campos-Olivas, I. Horr, C. Bormann, G. Jung, A.M. Gronenborn, Solution structure, backbone dynamics and chitin binding of the anti-fungal protein from Streptomyces tendae TU9011, J. Mol. Biol. 308 (2001) 765–782.
[8] A.K. Srivastava, Y. Sharma, K.V. Chary, A natively unfolded betagamma-crystallin domain from Hahella chejuensis1, Biochemistry 49 (2010) 9746–9755.
[9] A.K. Srivastava, Y. Sharma, K.V. Chary, Overexpression, on-column refolding and isotopic labeling of Hahellin from Hahella chejuensis, a putative member of the betagamma-crystallin superfamily4, Protein Expr. Purif. 58 (2008) 269–274.
[10] A.K. Srivastava, Y. Sharma, K.V. Chary, Sequence specific 1H, 13C, and 15N resonance assignments of Hahellin from Hahella chejuensis, a putative member of the betagamma-crystallin superfamily 3, Biomol. NMR Assign. 2 (2008) 151–153.
[11] H.S. Atreya, S.C. Sahu, K.V. Chary, G. Govil, A tracked approach for automated NMR assignments in proteins (TATAPRO)1, J. Biomol. NMR 17 (2000) 125–136.

[12] David S. Raiford, Cherie L. Fisk, Edwin D. Becker, Calibration of methanol and ethylene glycol nuclear magnetic resonance thermometers, Anal. Chem. 51 (1979) 2050–2051.
[13] P. Schanda, V. Forge, B. Brutscher, HET-SOFAST NMR for fast detection of structural compactness and heterogeneity along polypeptide chains, Magn. Reson. Chem. 44 Spec No (2006) S177–S184.
[14] L.E. Kay, D.A. Torchia, A. Bax, Backbone dynamics of proteins as studied by 15N inverse detected heteronuclear NMR spectroscopy: application to staphylococcal nuclease4, Biochemistry 28 (1989) 8972–8979.
[15] R.W. Creekmore, C.N. Reilley, Nuclear magnetic resonance determination of hydration numbers of electrolytes in concentrated aqueous solutions, J. Phys. Chem. 73 (1969) 1563–1568.
[16] N.A. Farrow, O. Zhang, A. Szabo, D.A. Torchia, L.E. Kay, Spectral density function mapping using 15N relaxation data exclusively2, J. Biomol. NMR 6 (1995) 153–162.
[17] J.F. Lefevre, K.T. Dayie, J.W. Peng, G. Wagner, Internal mobility in the partially folded DNA binding and dimerization domains of GAL4: NMR analysis of the N-H spectral density functions1, Biochemistry 35 (1996) 2674–2686.
[18] M.P. Williamson, Many residues in cytochrome c populate alternative states under equilibrium conditions4, Proteins 53 (2003) 731–739.
[19] N.J. Baxter, L.L. Hosszu, J.P. Waltho, M.P. Williamson, Characterisation of low free-energy excited states of folded proteins, J. Mol. Biol. 284 (1998) 1625–1639.
[20] H. Krizova, L. Zidek, M.J. Stone, M.V. Novotny, V. Sklenar, Temperature-dependent spectral density analysis applied to monitoring backbone dynamics of major urinary protein-I complexed with the pheromone 2-sec-butyl-4,5-dihydrothiazole7, J. Biomol. NMR 28 (2004) 369–384.